

1  
2  
3  
4  
5  
6  
7  
8  
9  
10  
11

# A Novel Liquid Biopsy-Based Approach for Highly Specific Cancer Diagnostics: Mitigating False Responses in Assaying Patient Plasma-Derived Circulating microRNAs through Combined SERS and Plasmon-Enhanced Fluorescence Analyses

12  
13  
14  
15  
16

Adrianna N. Masterson,<sup>a,#</sup> Thakshila Liyanage,<sup>a,#</sup> Claire Berman,<sup>a</sup> Hristos Kaimakliotis,<sup>b</sup> Merrell  
Johnson,<sup>c</sup> and Rajesh Sardar<sup>\*,a,s</sup>

17  
18  
19

<sup>a</sup>Department of Chemistry & Chemical Biology, Indiana University-Purdue University  
Indianapolis, 402 N. Blackford Street, Indianapolis, Indiana 46202, United States

20  
21  
22  
23

<sup>b</sup>Department of Urology, Indiana University School of Medicine, 535 N. Barnhill Dr.  
Indianapolis, Indiana 46202, United States

24  
25  
26

<sup>c</sup>Department of Physics, Purdue University Fort Wayne, 2101 E. Coliseum Blvd.  
Fort Wayne, Indiana 46805, United States

27  
28  
29  
30

<sup>s</sup>Integrated Nanosystems Development Institute, Indiana University-Purdue University  
Indianapolis, 723 W. Michigan Street, Indianapolis, Indiana 46202, United States

31  
32  
33  
34  
35

<sup>#</sup>These authors contributed equally to this work.

36  
37  
38  
39  
40

**KEYWORDS:** surface enhanced Raman scattering, plasmon-enhanced fluorescence, multimodal  
assay, microRNAs, gold triangular nanoprisms, liquid biopsy, point-of-care diagnostic

41  
42  
43  
44  
45  
46  
47  
48  
49  
50  
51  
52  
53  
54  
55

---

This is the author's manuscript of the article published in final edited form as:

Masterson, A. N., Liyanage, T., Berman, C., Kaimakliotis, H., Johnson, M., & Sardar, R. (2020). A novel liquid biopsy-based approach for highly specific cancer diagnostics: Mitigating false responses in assaying patient plasma-derived circulating microRNAs through combined SERS and plasmon-enhanced fluorescence analyses. *The Analyst*, 145(12), 4173–4180. <https://doi.org/10.1039/d0an00538j>

1  
2  
3 **One sentence text:** Novel multimodal assay has been developed to quantify circulating  
4 microRNAs through a combined surface-enhanced Raman scattering and plasmon-enhanced  
5 fluorescence approach  
6  
7  
8  
9  
10

11 **Abstract:**  
12

13  
14 Studies have shown that microRNAs, which are small noncoding RNAs, hold tremendous  
15 promise as next-generation circulating biomarkers for early cancer detection via liquid biopsies.  
16 A novel, solid-state nanoplasmonic sensor capable of assaying circulating microRNAs through a  
17 combined surface-enhanced Raman scattering (SERS) and plasmon-enhanced fluorescence  
18 (PEF) approach has been developed. Here, the unique localized surface plasmon resonance  
19 properties of chemically-synthesized gold triangular nanoprisms (Au TNPs) are utilized to create  
20 large SERS and PEF enhancements. With careful modification to the surface of Au TNPs, this  
21 sensing approach is capable of quantifying circulating microRNAs at femtogram/microliter  
22 concentrations. Uniquely, the multimodal analytical methods mitigate both false positive and  
23 false negative responses and demonstrate the high stability of our sensors within bodily fluids.  
24 As a proof of concept, microRNA-10b and microRNA-96 were directly assayed from the plasma  
25 of six bladder cancer patients. Results show potential for a highly specific liquid biopsy method  
26 that could be used in point-of-care clinical diagnostics to increase early cancer detection or any  
27 other diseases including SARS-CoV-2 in which RNAs can be used as biomarkers.  
28  
29  
30  
31  
32  
33  
34  
35  
36  
37  
38  
39  
40  
41  
42  
43  
44  
45  
46  
47  
48  
49  
50  
51  
52  
53  
54  
55  
56  
57  
58  
59  
60

## Introduction

Liquid biopsies involve analyzing circulating biomolecules in bodily fluids provide many advantages over traditional tissue biopsies for detecting cancers at an early stage as they are non-invasive, less expensive, and simpler.<sup>1</sup> Small non-coding RNAs, known as microRNAs, have been found to regulate a large number of human genes and play a significant role in various cancer developments.<sup>2-7</sup> Many studies have demonstrated that the detection of circulating microRNAs at an early stage, via liquid biopsies, could allow better treatment in an effort to prevent cancer progression and metastasis, increasing the chance of patient survival. The current “gold-standard” microRNA assays (i.e., quantitative reverse-transcription polymerase chain reaction (qRT-PCR)-based technologies) are capable of measuring microRNA levels reproducibly from bodily fluids in real-life clinical samples. However, this technology has several drawbacks including: (1) the treatment of biological fluid, (2) complicated labor-intensive RNA extraction, (3) required labeling and amplification prior to analysis, (4) complementary DNA conversion steps, and (5) the large volume of patient samples needed.<sup>8</sup> Together, these traits hinder translation into clinical point-of-care (POC) diagnostics.

In contrast, solid-state, label-free biosensing offers many unique advantages over qRT-PCR techniques, including simple sensor fabrication, high sensitivity, easy to miniaturization (of particular importance when adapting technologies to POC diagnostics), and elimination of receptor tagging with dyes or other specialized reagents (“label-free”). Among advantages, the latter is extremely important as it avoids undesirable interactions between labels and analytes, leading to more reliable and reproducible results. Current solid-state, label-free biosensing techniques such as microarray,<sup>9</sup> electrochemical,<sup>10, 11</sup> localized surface plasmon resonance (LSPR)-,<sup>12-14</sup> surface-enhanced Raman scattering (SERS)-,<sup>15, 16</sup> and photonic microring resonator-based<sup>17</sup> microRNA sensors provide good sensitivity. These single-mode detection methods rely on a specific sensing mechanism. For example, LSPR-based methods detect changes in local refractive index of the nanostructures while electrochemical-based measurements detect changes in current. Unfortunately, such changes can also result from non-specific adsorption of endogenous biomolecules from bodily fluids onto the sensor, as well as

1  
2  
3 structural changes that can be induced following placement within bodily fluids during the  
4 measurements. As a result, these techniques suffer from low specificity, particularly when  
5 analyzing bodily fluids, and can in turn produce false test results. Further, aside from  
6 detecting/analyzing the specific signal change that occurs from the analyte, no additional  
7 confirmation of analyte attachment to the sensor can be obtained. Among these techniques,  
8 SERS-based biomolecular assays are capable of using Raman signal to provide rich structural  
9 information on the analytes. However, current solid-state SERS-based microRNA assays still  
10 show many problems, including low sensitivity, poor specificity, and inability to analyze real-life  
11 patient samples.<sup>15, 16, 18-21</sup>

12  
13  
14  
15  
16  
17  
18  
19 High specificity is the most crucial factor in creating assays that can avoid false-positive  
20 and/or false-negative test results for the POC diagnosis.<sup>22, 23</sup> To overcome the current  
21 technological bottleneck in real-life patient sample analysis, we present, for the first time, the  
22 design of a solid-state nanoplasmonic sensor. This novel sensing approach is capable of assaying  
23 oncogenic microRNAs directly in human plasma with high sensitivity and specificity. Here, the  
24 unique LSPR properties<sup>24, 25</sup> of noble metal nanoparticles are utilized for the detection of  
25 microRNAs via a combined SERS<sup>26, 27</sup> and plasmon-enhanced fluorescence (PEF)<sup>28, 29</sup> approach.  
26 Importantly, the same nanoplasmonic sensor can be used in this multimodal detection method;  
27 no changes to structural parameters are required. To demonstrate the potential translational  
28 aspects of our dual detection technique in liquid biopsies for POC diagnosis, we successfully  
29 assayed two oncogenic microRNAs (microRNA-10b and microRNA-96). Analysis was  
30 performed directly in six bladder cancer patient plasma samples at sub-femtogram/microliter  
31 (fg/ $\mu$ L) concentrations.  
32  
33  
34  
35  
36  
37  
38  
39  
40  
41  
42  
43  
44  
45  
46  
47  
48  
49  
50  
51  
52  
53  
54  
55  
56  
57  
58  
59  
60

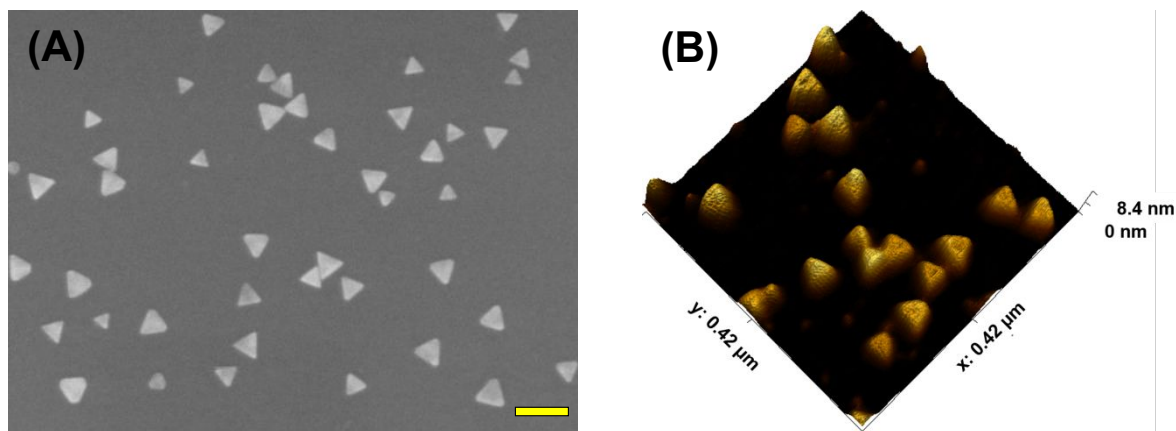


**Fig. 1. Structural characterizations of Au TNPs.** (A) A representative scanning electron microscopy image of Au TNPs attached onto a silanized glass substrate. Scale bar is 100 nm. (B) An atomic force micrograph of Au TNPs.

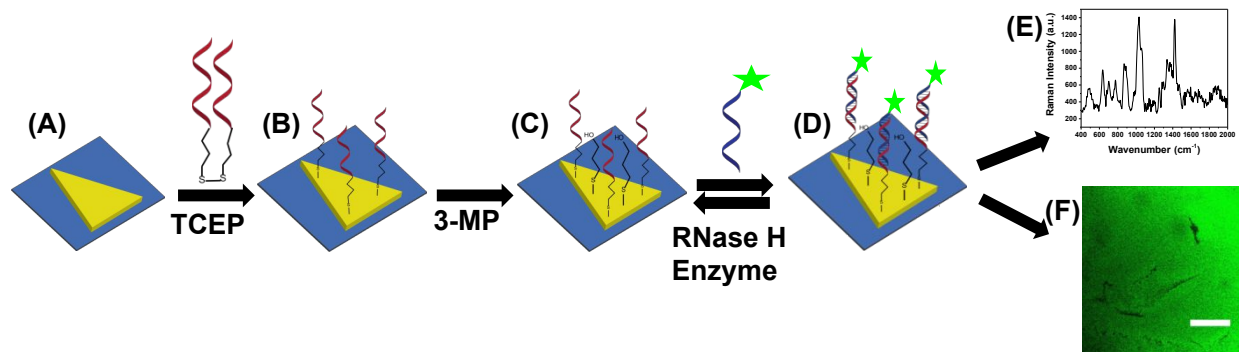


**Figure 2. Design of a nanoplasmonic sensor for the detection of microRNAs using combined surface-enhanced Raman spectroscopy (SERS) and fluorescence confocal microscopy techniques.** (A) Freshly synthesized Au TNPs were attached onto silanized glass coverslip. (B) Tris(2-carboxyethyl) phosphine (TCEP) addition to DNA-disulfide solution breaks disulfide bonds and subsequent incubation in the solution resulted in the attachment of -ssDNAs on the surface of TNPs. Generally, -ssDNAs were randomly organized on the flat metal surface (e.g., here TNPs).<sup>10</sup> (C) -ssDNA-attached Au TNPs were further functionalized with 3-mercaptopropanol (3-MP) to allow -ssDNAs to “stand up” to achieve the most favorable -ssDNA/microRNA hybridization. The functionalization steps until (C) produced nanoplasmonic sensors, where microRNA-10b/96-FAM can selectively bind (D) to be analyzed by both SERS spectroscopy (E) and fluorescence confocal microscopy (F). Nanoplasmonic sensors can also be regenerated by incubating microRNA-bound sensors in a RNase H enzyme solution; image not to scale.

## Experimental Section

**Materials.** Chloro(triethylphosphine) gold(I) ( $\text{Et}_3\text{PAuCl}$ , 97%) was purchased from Gelest Inc. Poly-(methylhydrosiloxane) (PMHS,  $M_n = 1700\text{--}3300$ ), triethylamine (TEA, 98%), ACS grade acetonitrile ( $\text{CH}_3\text{CN}$ , 99.9%), and 3-mercaptopropanol (3-MP, 95%) were purchased from Sigma-Aldrich. Thiol modified 5'-SH-( $\text{CH}_2$ )<sub>3</sub>-ssDNAs, and various microRNAs were purchased from Integrated DNA Technologies (IDT). RNase H enzyme and RBS detergent solution were

1  
2  
3 purchased from Thermo Scientific. (3-Mercaptopropyl)-trimethoxysilane (MPTMS, 94%) was  
4 purchased from Alfa Aesar. All the chemicals were used without any further purifications.  
5 RNase free sterile water was obtained from Baxter Healthcare Corporation. The glass cover slips  
6 and the tris(2-carboxyethyl)phosphine (TCEP) solution were purchased from Fisher Scientific.  
7 Bladder cancer patient plasma samples were obtained from the Indiana University medical  
8 school and used as received. All water was purified using a Thermo Scientific Barnstead  
9 Nanopure system. Thiol modified -ssDNAs, microRNAs were stored at  $-80\text{ }^{\circ}\text{C}$ . PBS buffer (pH  
10 = 7.2) was prepared using RNase-free sterile water. All experiments were performed in  
11 accordance with the Guidelines of the United States and approved by the ethics committee at  
12 Indiana University. Informed consents were obtained from human participants of this study.  
13  
14  
15  
16  
17

18  
19 **Fabrication of Nanoplasmonic Sensors.** Gold triangular nanoprisms (Au TNPs) were  
20 synthesized using our well-established method.<sup>12, 14, 30</sup>  $\text{Et}_3\text{PAu(I)Cl}$  (10 mg) was dissolved in 20  
21 mL of acetonitrile. After five minutes of stirring at room temperature, 0.019 mL (0.136 mmol)  
22 TEA was added, and the mixture was heated to  $40\text{ }^{\circ}\text{C}$ . Then, 0.3 mL (2.75 mmol) of PMHS was  
23 added, and the reaction ran until the desired LSPR peak of 800 nm was achieved. Au TNPs were  
24 then attached onto silanized glass coverslips as we reported previously.<sup>13</sup> Separately, a mixture  
25 of  $5\text{ }\mu\text{M}$  -C3-ssDNA-10b/96 with 0.1 M TCEP was prepared and allowed to react for 1 hour to  
26 break disulfide bonds. The solution was then diluted with PBS buffer, and the resulting solution  
27 was used to incubate Au TNPs for overnight. The addition of -ssDNA-10/96 solutions induced  
28 ligand exchange of Au TNPs by removing TEA and PMHS that were present on the surface  
29 during the colloidal synthesis. Next, -ssDNA-10b/96-functionalized Au TNPs were washed  
30 thoroughly with RNase free water, and both UV-Vis spectrum and Raman spectrum were  
31 acquired. Finally, 10 mL, 1.0 mM 3-MP solution was added to ssDNA-10b/96-functionalized Au  
32 TNPs to fabricate nanoplasmonic sensors. Various concentrations (100 nM – 100 fM) of  
33 microRNA-10b or microRNA-96 in 10 mL PBS buffer were used to incubate nanoplasmonic  
34 sensors for 2 hours. MicroRNA bound nanoplasmonic sensors were washed thoroughly with  
35 RNase free water to remove any loosely bound microRNAs to the sensor. For the  
36 reversibility/regeneration tests, microRNA-bound nanoplasmonic sensors were incubated in 15  
37 units RNase H enzyme in RNase free water for 2 hours.  
38  
39  
40  
41  
42  
43  
44  
45  
46  
47  
48  
49  
50

51  
52 **UV-Vis and SERS measurements, and fluorescence confocal microscopy imaging.** UV-Vis  
53 spectra were collected from 1100–300 nm on a Varian Cary 50 UV/Vis spectrophotometer, and  
54 all sensors were analyzed in RNase free water. SERS spectra were collected of the sensor on  
55  
56  
57  
58  
59  
60

1  
2  
3 clean aluminum foil using a Foster-FORAM 785 HP Raman spectrometer with a 785 nm diode  
4 laser excitation source. Samples were placed on top of the aluminum foil when analyzed due to  
5 the requirement of a clean surface to analyze. The background scan was taken of a polystyrene  
6 bead to calibrate the laser. For all SERS measurements, two randomly selected spots were  
7 analyzed for each sensor and for three-separate sensors (a total of six measurements). Using a  
8 Fluoview FV1000 MPE laser scanning biological microscope, 100 nM Alexa-488 dye was used  
9 in the analysis of the sensors. A laser power of 40%, a 60x water objective, and gain of 1x were  
10 used for the image acquisition. The diameter of the laser spot was 5- $\mu$ M.

11  
12 **Scanning Electron and Atomic Force Microscopy Analyses.** The chemically synthesized Au  
13 TNPs attached onto the silanized glass coverslips were characterized by scanning electron  
14 microscopy (SEM) and atomic force microscopy (AFM). SEM micrographs were obtained using  
15 a Hitachi S-4700 Field Emission Scanning Electron Microscope (FESEM) at 20 kV accelerating  
16 voltage, and AFM images were obtained using a Bioscope AFM instrument.

17  
18 **Construction of Calibration Curves.** All SERS spectra were baseline corrected using OMNIC  
19 software. The Fit Peaks tool was used in Origin 2018b to find peak intensity with Lorentz fitting.  
20 Peak intensity at a specific wavenumber was graphed as a function of concentration. Linear  
21 fitting was used to find the R-squared value.

22  
23 **Measuring False Responses.** In order to demonstrate the efficiency of our solid-state  
24 nanoplasmonic-based sensors mitigating false responses, we analyzed the patient samples that  
25 measured the highest and lowest concentrations. Nanoplasmonic-based sensors, which were  
26 used to quantify microRNA-10b/96 in patient plasma again re-incubated in 15 units RNase H  
27 enzyme in RNase free water for 2 h. Next, both SERS measurement fluorescence confocal  
28 measurements were performed. Again, the same sensors were incubated in a 100 nM solution of  
29 microRNA-FAM. After the sensors were thoroughly washed with RNase free water, SERS and  
30 fluorescence analyses were conducted.

## Results and Discussion

To acquire both SERS and PEF signals from the same nanoplasmonic sensor, we used chemically-synthesized gold triangular nanoprisms (Au TNPs) to generate high intensity LSPR.<sup>31</sup> This intensified LSPR arises due to strong electromagnetic field (EM) enhancement that occurs at the sharp tips and edges of Au TNPs.<sup>32-35</sup> This leads to the formation of hot-spots, which are ideal for LSPR-based SERS and PEF mechanisms.<sup>26, 29</sup> For the first time, we have utilized PEF to unequivocally confirm microRNA attachment onto the nanoplasmonic sensor by utilizing fluorescence confocal imaging. Together, these methods fully eliminate the possibility of false assay responses. Further, in addition to their unique LSPR properties, the atomically flat Au TNPs allow -ssDNAs to form a tightly-packed self-assembled monolayer (SAM) on their surface, allowing for high reproducibility throughout the sensor. This is important in the context of making good interactions and forming a -ssDNA/microRNA duplex. Moreover, tightly-packed SAMs avoid non-specific adsorption of biomolecules onto the Au surface. Au is also extremely stable in human biofluids, therefore sensors are expected to maintain excellent structural integrity. Taking into consideration all their unique structural properties, we chose to Au TNPs with a 42 and 8 nm edge length and thickness, respectively, for the fabrication of our nanoplasmonic sensors, as shown in **Fig. 1**.

The fabrication of nanoplasmonic sensors is illustrated in **Fig. 2**, where : (A) Au TNPs were chemically-attached onto silanized glass substrate; (B) TNPs were functionalized with -ssDNA-(10b/96) via the Au-S bond, and in order to increase their specificity in SERS, they were further functionalized with 3-mercaptopropyl (3-MP) (**Fig. 2C**) so that the -ssDNA-10b/96 would appear in a “standup” position. This standup formation creates an ideal distance between the fluorophore and Au TNPs to maximize PEF enhancement by reducing fluorescence quenching through the Förster resonance energy transfer (FRET) process. In addition, stand-up -ssDNAs provides adequate space for the microRNAs to form -ssDNA/microRNA duplexes. Finally, 3-MP also improves specificity, as reported in the literature.<sup>10</sup> The functionalizations of Au TNPs with -ssDNA-(10b/96) and 3-MP represent our nanoplasmonic sensors. **Fig. 2D** shows attachment of a fully complementary microRNA tagged with a 6-fluorescein (FAM), allowing complete -ssDNA/microRNA-FAM hybridization. Most importantly, as shown in **Fig. 2D**, the nanoplasmonic sensors are fully reversible and regenerative to allow use for multiple analyses.



1  
2  
3 This is critical in the context of determining sensor stability and showing that they maintain  
4 complete structural integrity during assays.  
5  
6

7        Attachment of microRNA-FAM to the nanoplasmonic sensor can be detected/confirmed  
8 utilizing both SERS (**Fig. 2E**) and fluorescence confocal microscopy (**Fig. 2F**) techniques. It is  
9 important to highlight the additional advantages of selecting this particular dimension Au TNP  
10 for a SERS-based microRNA assay: (1) As shown in **Fig. S1**, the LSPR peak position of  
11 nanoplasmonic sensors is  $\sim 860$  nm. The LSPR peak of TNPs and the wavelength of incident  
12 laser light controls the intensity of hot-spots. Ideally, for the EM-field-driven SERS  
13 enhancement, the LSPR wavelength of nanostructures in the sensors should be longer than the  
14 wavelength of laser light; (2) Use of a low energy laser (e.g., 785 nm) that fits the excitation  
15 requirements for nanostructures is important for biosensing applications in order to avoid  
16 degradation of biomolecules, particularly microRNAs.  
17  
18  
19  
20  
21  
22  
23  
24

25        Each step in the fabrication of these nanoplasmonic sensors was characterized through  
26 SERS spectroscopy (see **Fig. 3**). Attachment of -ssDNA-(10b/96) via Au-S bonds results in the  
27 appearance of a C-S Raman stretch at  $635\text{ cm}^{-1}$ . Furthermore, several new Raman stretches that  
28 are characteristic of DNAs (see **Fig. 3A and Fig. S2**) such as guanine (G) ring breathing at  $688$   
29  $\text{cm}^{-1}$ , adenine ring breathing at  $733\text{ cm}^{-1}$ , cytosine ring breathing at  $790\text{ cm}^{-1}$ , and the  
30 phosphodiester group of the nucleic acids at  $1289\text{ cm}^{-1}$  are also observed.<sup>18, 21, 36-38</sup> The C-H  
31 Raman stretch at  $1400\text{ cm}^{-1}$  further confirms the functionalization of Au TNPs with 3-MP  
32 (Figure 3A-blue).<sup>39</sup> Incubation of microRNA-(10b/96)-FAM to the nanoplasmonic sensor  
33 displays a prominent Raman peak at  $1062\text{ cm}^{-1}$  of the additional  $\text{PO}_2^-$  symmetrical stretch.<sup>38</sup>  
34 Furthermore, the Raman stretch at  $1255\text{ cm}^{-1}$  corresponds to guanine C8-H bending<sup>18, 21, 36, 37</sup> and  
35 the low intensity Raman stretch at  $1645\text{ cm}^{-1}$  is unique to the uracil C=O stretch.<sup>18, 21, 36, 37</sup> **Fig.**  
36 **3B** illustrates SERS spectra of the microRNA-10b varying concentrations from 100 nanomolar  
37 (nM) to 100 femtomolar (fM).  
38  
39  
40  
41  
42  
43  
44  
45  
46  
47

48        The average edge-length of our chemically synthesized Au TNPs is 42 nm that provides a  
49 top surface area of  $764\text{ nm}^2$ . Considering all the -ssDNA probes were attached onto the top  
50 surface and thiolate has a  $0.25\text{ nm}^2$  footprint, there would be approximately 3000 -ssDNA-  
51 (10b/96) attached per TNP. In the nanoplasmonic sensors fabrication, we used a high  
52 concentration of 3-MP in comparison to -ssDNA probes. Therefore, the -ssDNA grafting density  
53  
54  
55  
56  
57  
58  
59  
60

is overestimated because a relatively large percentage of TNP surface would be occupied by 3-MP molecules. Further experimental characterization is required to quantitatively determine the grafting density of -ssDNA probe that is currently under our investigation.

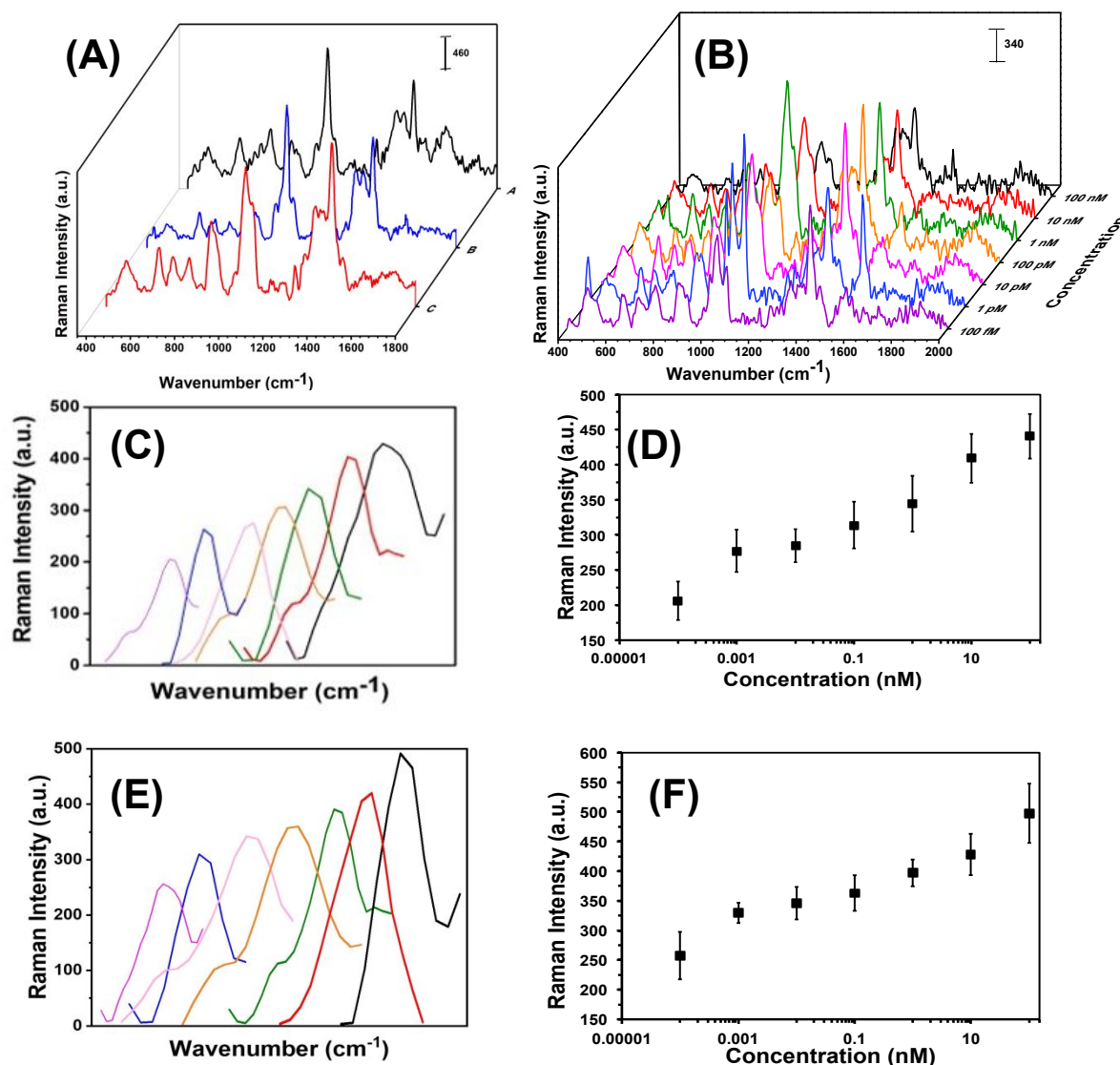


**Fig. 3. The SERS-based microRNA assay using nanoplasmonic sensors. (A)** SERS spectra at different stages: Functionalization of AuNPs with -ssDNA-10b, A; after attachment of 3-MP on TNPs, B; and after incubation of nanoplasmonic sensors in a microRNA-10b solution, C. **(B)** SERS spectra of nanoplasmonic sensors upon incubation in different concentrations of microRNA-10b solution. **(C)** Expanded SERS spectra of the C8-H bending stretch of Guanine at 1255 cm<sup>-1</sup> in various microRNA-10b concentrations (light purple: 100 fM, blue: 1 pM, pink: 10 pM, orange: 100 pM, green: 1 nM, red: 10 nM,

1  
2  
3 black: 100 nM). **(D)** Intensity of the C8-H bending stretch at  $1255\text{ cm}^{-1}$  as a function of microRNA-10b  
4 concentration (logarithmic scale).  $Y = 15.94 \ln(X) + 361.88$ ,  $R^2 = 0.97$ . **(E)** Expanded SERS spectra of  
5 the C8-H bending stretch of Guanine at  $1255\text{ cm}^{-1}$  in various microRNA-96 concentrations (light purple:  
6 100 fM, blue: 1 pM, pink: 10 pM, orange: 100 pM, green: 1 nM, red: 10 nM, black: 100 nM). **(F)**  
7 Intensity of the C8-H bending stretch at  $1255\text{ cm}^{-1}$  as a function of microRNA-96 concentration  
8 (logarithmic scale).  $Y = 15.04 \ln(X) + 408.73$ ,  $R^2 = 0.95$ . In C and E, the individual concentrations of the  
9 microRNA calibration curve are plotted in order to better visualize of the increase in intensity. Each  
10 spectrum has the same wavenumber of  $1255\text{ cm}^{-1}$  and does not shift in wavenumber as seen in the figure.  
11

12 In literature, researchers have used a variety of SERS stretches to develop the calibration  
13 plots for microRNA assays, but have done so without providing any detailed rationale for their  
14 selections.<sup>16, 19, 40</sup> Theoretical calculations show that the C8-H bending Raman stretch of guanine  
15 at  $1255\text{ cm}^{-1}$  could be ideal to develop the calibration plot,<sup>41</sup> thus we selected this SERS stretch  
16 for our studies. As shown in **Fig. 3C and E** for microRNA-10b and microRNA-96, respectively,  
17 a continuous increase in C8-H stretch intensity is displayed when corresponding nanoplasmonic  
18 sensors were incubated in various concentrations of microRNA solution. The SERS intensity of  
19 the C8-H bending mode versus the concentration of microRNAs is appeared to be linear over the  
20 entire concentration range (**Fig. 3D and F, Table S3 and Table S4**). The limit of detections  
21 (LODs) for microRNA-10b and microRNA-96 calibration was calculated using a published  
22 method that follows:<sup>40, 42</sup>  
23  
24  
25  
26  
27  
28  
29  
30

$$\text{LOD} = 10^{3m/k} \text{fM}$$

31  
32 Here,  $m$  is the relative standard deviation of the blank and  $k$  is the slope of the SERS intensity  
33 versus microRNA on the concentration curve. Our LODs for microRNA-10b and microRNA-96  
34 are calculated at 1.13 pM and 0.030 pM, respectively. Importantly, this represents a 10-fold  
35 improved LODs in comparison to previously reported SERS-based microRNA assays.<sup>38</sup> We  
36 believe that the high SERS sensitivity of our nanoplasmonic sensors is due the intensified  
37 hotspots at the sharp tips and edges of the Au TNPs, as previously shown through discrete dipole  
38 approximation calculations.<sup>32-34</sup>  
39  
40  
41  
42  
43  
44  
45  
46  
47  
48  
49  
50  
51  
52  
53  
54  
55  
56  
57  
58  
59  
60

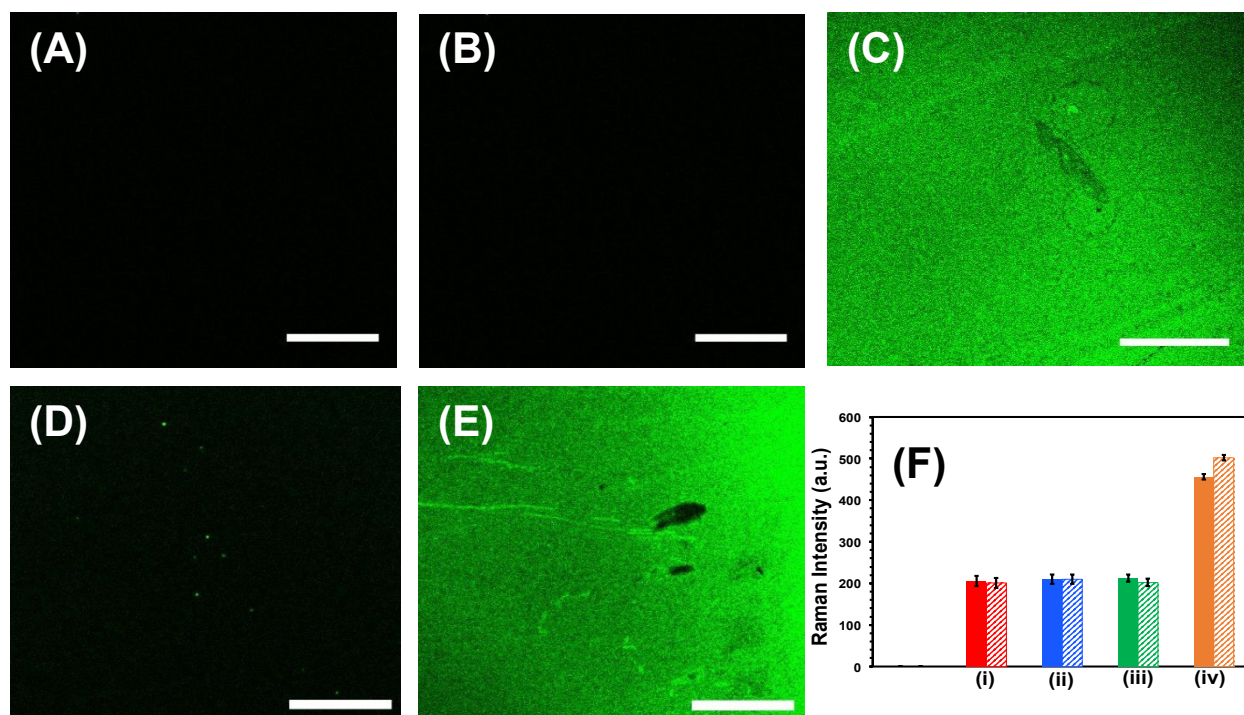


**Fig. 4: Specificity tests of nanoplasmonic sensors for the microRNA detection.** Fluorescence confocal microscopy images of (A) glass substrate attached Au TNPs, (B) mixed -ssDNA-10b and 3-MP functionalized Au TNPs (nanoplasmonic sensor), (C) After incubation of nanoplasmonic sensors in a 100 nM microRNA-10b-FAM solution, (D) After treatment of nanoplasmonic sensors with RNase H enzyme to regenerate the sensor, (E) After re-incubation of nanoplasmonic sensors in a 100 nM microRNA-10b-FAM solution. Scale bars are 50  $\mu\text{m}$ . (F) Normalized Intensity of the C8-H bending stretch at  $1255\text{ cm}^{-1}$  for two different microRNAs (solid bars, microRNA-10b; dashed bars, microRNA-96). Black bars represent glass substrate attached AuNPs (not visible). (i) Red bars represent mixed -ssDNA-10b and 3-MP functionalized Au TNPs or -ssDNA-96 and 3-MP functionalized Au TNPs. (ii) Blue bars represent incubation of nanoplasmonic sensor in a control patient (without the history of cancer) plasma. Green bars represent incubation of nanoplasmonic sensors in a mixture of microRNA-96, 145, 143, and 490-5p solution for the -ssDNA-10b functionalized Au TNPs, or a mixture of microRNA-10b, 145, 143, 490-5p solution for the -ssDNA-96 functionalized Au TNPs. These microRNAs are non-complementary to either -ssDNA-10b or -ssDNA-96. Orange bars represent incubation of nanoplasmonic sensors either in 100 nM microRNA-10b or microRNA-96 solution.

Successful implementation of the developed biosensors in liquid biopsy-based cancer diagnostics requires unprecedentedly high specificity, specifically to avoid false test results.<sup>1</sup> First, the specificity, which is the ability to unambiguously identify the analyte of our nanoplasmonic sensors, was investigated through fluorescence confocal imaging of labeled target microRNAs. We used microRNA-10b as a model system to study the specificity of the nanoplasmonic sensors. **Fig. 4A** confirms that our nanoplasmonic sensors do not display any

1  
2  
3 fluorescence (in the absence of microRNAs). Similarly, when Au TNPs were functionalized only  
4 with 3-MP (without -ssDNA-10b) and then incubated in a microRNA-10b-FAM solution, no  
5 fluorescence signals are detected (data not shown). Further, when the 3-MP functionalized Au  
6 TNPs were incubated in a -ssDNA-10b solution, no fluorescence is detected (**Fig. 4B**). However,  
7  
8 when the nanoplasmonic sensors, which were constructed to detect microRNA-10b, were  
9  
10 incubated in a microRNA-10b-FAM solution followed by copious rinsing, confocal imaging  
11  
12 shows bright green fluorescence (**Fig. 4C**). Additionally, a control experiment was performed by  
13  
14 incubating a MPTMS functionalized glass coverslip in -ssDNA and microRNA directly without  
15  
16 the presence of Au TNPs. The obtained SERS and fluorescence signals showed no results (data  
17  
18 not shown). These experimental data suggest the formation of a -ssDNA-10b/microRNA-10b-  
19  
20 FAM duplex. Metallic nanostructures are capable of enhancing fluorescence signal through the  
21  
22 PEF mechanism, in which LSPR properties of the nanostructure increase the radiative decay rate  
23  
24 of the fluorophore.<sup>43</sup> To reduce fluorescence quenching due to FRET processes between the  
25  
26 nanostructure and fluorophore, it is important that the fluorophore resides within a particular  
27  
28 distance from the metal surface. Recent studies showed that a distance of 7.0 to 16.2 nm,  
29  
30 corresponding to 18 to 45 nucleotides, between Au nanostructures and fluorophores provides the  
31  
32 strongest fluorescence enhancement.<sup>28</sup> Importantly, microRNA-10b contains 23 nucleotides and  
33  
34 thus the spacing between FAM molecules and Au TNPs is within the reported distance for  
35  
36 highest fluorescence enhancement. To further confirm our confocal-based imaging results,  
37  
38 which demonstrate that nanoplasmonic sensors unambiguously detect microRNAs with high  
39  
40 specificity, we incubated microRNA-10b-FAM-attached nanoplasmonic sensors in a RNase H  
41  
42 enzyme solution. This solution is expected to break the -ssDNA/microRNA duplex, removing  
43  
44 the attached microRNA, to regenerate the original sensor. As predicted, following RNase H  
45  
46 incubation, the fluorescence signal completely disappears, as shown in **Fig. 4D**. As illustrated in  
47  
48 **Fig. 4E**, the fluorescence signal reappears when sensors were again incubated in then  
49  
50 microRNA-10b-FAM solution. These results show the fully regenerative capabilities of the  
51  
52 developed nanoplasmonic sensors. Sensor regeneration was further confirmed by the decrease or  
53  
54 increase of the 1255 cm<sup>-1</sup> peak of the C8-H bending mode in the SERS spectra after -ssDNA-10b  
55  
56 attachment, 3-MP attachment, microRNA-10b-FAM attachment, incubation in RNase H enzyme,  
57  
58 and re-incubation in microRNA-10b-FAM (**Fig. S3**).

1  
2  
3  
4  
5  
6  
7  
8  
9  
10  
11  
12  
13  
14  
15  
16  
17  
18  
19  
20  
21  
22  
23  
24  
25  
26  
27  
28  
29  
30  
31  
32  
33  
34

Next, we investigated the specificity of our label-free assay for microRNA-10b and microRNA-96 detection using the SERS technique, as shown in **Fig. 4F** and **Fig. S4**. Here, the nanoplasmonic sensors, which are capable of detecting microRNA-10b, were incubated in a mixture of microRNA-96, microRNA-145, microRNA-143, and microRNA-490-5p. The levels of these microRNAs are commonly altered in patients with a history of bladder cancer.<sup>13</sup> SERS analysis shows that the intensity of the C8-H bending mode at  $1255\text{ cm}^{-1}$  does not increase when compared to the original nanoplasmonic sensors. This is because microRNA-96, microRNA-145, microRNA-143, and microRNA-490-5p are non-complementary to –ssDNA-10b. However, when the same nanoplasmonic sensor was incubated in the complimentary microRNA-10b solution, an increase in SERS intensity of the C8-H bending mode is observed. Thus, by measuring the Raman intensity in the presence of either non-complimentary/complementary microRNAs, we can unequivocally conclude the high specificity of our nanoplasmonic sensors towards targeted microRNAs. Taken together, our multimodal fluorescence and SERS analyses not only confirm the high specificity of the nanoplasmonic sensors towards the microRNA assay, but also demonstrate the reusability of the newly developed label-free technique. Sensor regeneration is a particularly an important aspect as the ability for repeated measurements not only provides unmatched accuracy, but also it is commercially important in low- and middle-income countries.

35  
36  
37  
38  
39  
40  
41  
42  
43  
44  
45  
46  
47  
48  
49  
50  
51  
52  
53  
54  
55  
56  
57  
58  
59  
60

To demonstrate the translational aspects of our newly developed technology for clinical POC cancer diagnostics, we successfully assayed two oncogenic microRNAs (microRNA-10b and microRNA-96) directly in plasma from metastatic bladder cancer patients. **Fig. 5A** demonstrates microRNA-10b and microRNA-96 levels in six patients. It should be noted that all patients were categorized in the metastatic stage; however, the level of microRNA varies from one to another. To mitigate false positive and false negative test results, we re-analyzed the two nanoplasmonic sensors that measured the highest (patient 2 shows a high microRNA-10b level that could arise from false positive response) and the lowest (patient 5 shows a low microRNA-10b level that could lead to false negative response) microRNA-10b concentrations. It is expected that both sensors that were incubated in the patient plasma containing – ssDNA/microRNA-10b duplexes. As shown in **Fig. 5B**, SERS intensities decrease following RNase H enzyme treatment. Re-incubation of the regenerated sensors into microRNA-10b-FAM results in nearly the same SERS intensity values, as shown in **Fig. 4F**. Finally, we also



characterized the nanoplasmonic sensor containing microRNA-10b-FAM by fluorescence confocal microscopy, which reveals excellent specificity (**Fig. 5C**). A similar SERS study was also conducted for microRNA-96 involving patient 3 and 6 (see **Fig. 5D**) as described for microRNA-10b.

To the best of our knowledge, this is the first example where a SERS-based technique has been successfully implemented in the microRNA assay of clinically relevant samples without any sample processing. Experimental data confirm that the developed nanoplasmonic sensors did not compromise sensitivity or specificity aspects upon incubation in patient plasma, and the concentrations that were determined are true values.

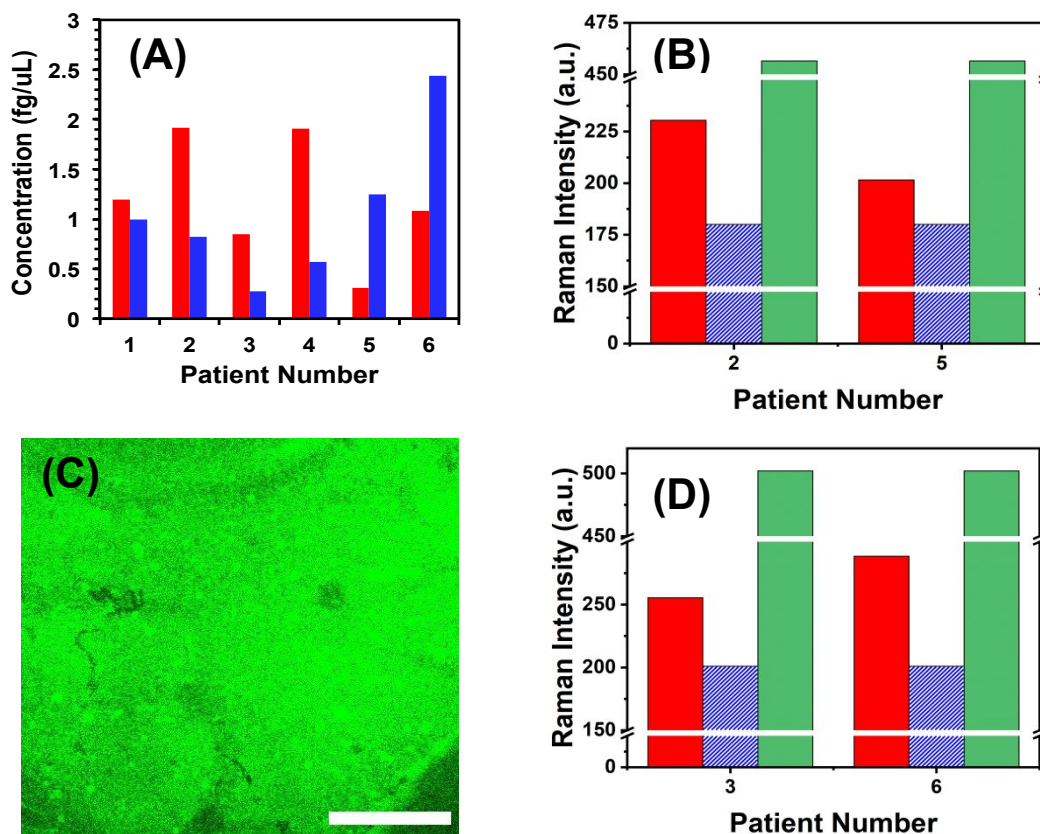


**Fig. 5. Nanoplasmonic sensor-based liquid biopsy for cancer detection.** (A) SERS-based microRNA quantification in six different bladder cancer-related patient plasma samples. microRNA-10b and microRNA-96 are shown in red and blue bars, respectively. (B) Examination of false test resulting by measuring SERS intensities for two different patients containing the highest (patient 2) and the lowest (patient 5) microRNA-10b levels. Red solid bars represent the Raman intensity of C8-H bending stretch at  $1255\text{ cm}^{-1}$ , blue dashed bars after regeneration of nanoplasmonic sensors through RNase H treatment, and green dotted bars are after incubation of nanoplasmonic sensors in  $100\text{ nM}$  microRNA-10b-FAM solution. (C) A representative fluorescence confocal image of the nanoplasmonic sensor after incubating

1  
2  
3 in 100 nM microRNA-10b-FAM solution. **(D)** Examination of false test resulting by measuring SERS  
4 intensities for two different patients containing the lowest (patient 3) and the highest (patient 6)  
5 microRNA-96 levels. The bars are color coordinated as shown in panel (B). Scale bars is 50  $\mu\text{m}$ .  
6  
7  
8  
9  
10

## 11 **Conclusion**

12  
13  
14 In conclusion, we have designed and fabricated SERS-based, highly sensitive, specific, and  
15 regenerative nanoplasmonic sensors for the first time. These sensors were capable of quantifying  
16 oncogenic microRNAs at sub-fg/ $\mu\text{L}$  concentrations directly from patient plasma, thus obviating  
17 the complications associated with current gold-standard qRT-PCR-based technologies. The  
18 unique LSPR properties of Au TNPs were utilized to achieve a combined dual-detection SERS  
19 and fluorescence analysis that allows mitigation of false test results. The newly developed,  
20 label-free microRNA assay technique has unmatched potential to expand SERS-based biomarker  
21 quantification in the early detection of cancers through liquid biopsies. Importantly, this holds  
22 promise in advancing POC clinical diagnostics, which could be performed using a  
23 handheld/portable Raman instrument. Taken together, we believe our multimodal, innovative  
24 detection approach, which has been validated using plasma from bladder cancer patients  
25 samples, should also be applicable to other cancers (e.g., colon, breast, prostate, and pancreatic)  
26 as well as various diseases (e.g., cardiovascular, Alzheimer, and infectious) that involve  
27 circulating nucleic acids (e.g., DNAs, long non-coding RNAs, and microRNAs) as biomarkers.<sup>8</sup>  
28  
29  
30  
31  
32  
33  
34  
35  
36  
37  
38

## 39 **Acknowledgements**

40  
41 This work is supported by the National Science Foundation, award number CBET-1604617. We  
42 thank Dr. Daniel Minner for valuable comments and suggestions. We would like to thank  
43 Indiana Clinical and Translational Sciences Institute, which was supported, in parts, by Award  
44 Number UL1TR002529 from the National Institutes of Health, National Center for Advancing  
45 Translational Sciences, Clinical and Translational Sciences Award.  
46  
47  
48  
49

50  
51 **Electronic Supplementary Information.** Detailed experimental procedures for Au TNPs  
52 synthesis, various spectroscopy and microscopy characterizations, and additional extinction and  
53 Raman spectra, and raw Raman data. These materials are available free of charge. (PDF)  
54  
55  
56  
57  
58  
59  
60



## AUTHOR INFORMATION

Corresponding Author

\*Rajesh Sardar; Email: rsardar@iupui.edu

## References

1. J. Das and S. O. Kelley, *Angewandte Chemie, International Edition*, 2020, **59**, 2554-2564.
2. D. P. Bartel, *Cell* 2004, **116**, 281-297.
3. A. Esquela-Kerscher and F. J. Slack, *Nature Reviews Cancer*, 2006, **6**, 259-269.
4. D. J. Lockhart and E. A. Winzeler, *Nature*, 2000, **405**, 827-836.
5. J. Lu, G. Getz, E. A. Miska, E. Alvarez-Saavedra, J. Lamb, D. Peck, A. Sweet-Cordero, B. L. Ebert, R. H. Mak, A. A. Ferrando, J. R. Downing, T. Jacks, H. R. Horvitz and T. R. Golub, *Nature* 2005, **435**, 834-838.
6. F. Petrocca and J. Lieberman, *RNA Biology*, 2009, **6**, 335-340.
7. J. Wang, J. Chen and S. Sen, *Journal of Cellular Physiology*, 2016, **231**, 25-30.
8. Z. Jin, D. Geißler, X. Qiu, K. D. Wegner and N. Hildebrandt, *Angewandte Chemie, International Edition*, 2015, **54**, 10024-10029.
9. S. Fang, H. J. Lee, A. W. Wark and R. M. Corn, *Journal of the American Chemical Society*, 2006, **128**, 14044-14046.
10. B. N. Johnson and R. Mutharasan, *Anal. Chem.* , 2012, **84**, 10426-10436.
11. M. Wanunu, T. Dadosh, V. Ray, J. Jin, L. McReynolds and M. Drndić, *Nat. Nanotech.*, 2010, **5**, 807-814.
12. G. K. Joshi, S. Deitz-McElyea, T. Liyanage, K. Lawrence, S. Mali, R. Sardar and M. Korc, *ACS Nano*, 2015, **9**, 11075-11089.
13. T. Liyanage, A. N. Masterson, H. H. Oyem, H. Kaimakliotis, H. Nguyen and R. Sardar, *Anal. Chem.* , 2019, **91**, 1894-1903.
14. G. K. Joshi, S. Deitz-McElyea, M. Johnson, S. Mali, M. Korc and R. Sardar, *Nano Letters*, 2014, **14**, 6955-6963.
15. D. Graham, B. J. Mallinder and W. E. Smith, *Angewandte Chemie, International Edition*, 2000, **39**, 1061-1063.
16. Y. C. Cao, R. Jin and C. A. Mirkin, *Science* 2002, **297**, 1536-1540.
17. A. J. Qavi and R. C. Bailey, *Angewandte Chemie, International Edition*, 2010, **49**, 4608-4611.
18. J. L. Abell, J. M. Garren, J. D. Driskell, R. A. Tripp and Y. Zhao, *Journal of the American Chemical Society*, 2012, **134**, 12889-12892.
19. J. D. Driskell and R. A. Tripp, *Chem. Commun.*, 2010, **46**, 3298-3300.
20. L. Qi, M. Xiao, X. Wang, C. Wang, L. Wang, S. Song, X. Qu, L. Li, J. Shi and H. Pei, *Anal. Chem.*, 2017, **89**, 9850-9856.
21. S. Tian, O. Neumann, M. J. McClain, X. Yang, L. Zhou, C. Zhang, P. Nordlander and N. J. Halas, *Nano Letters*, 2017, **17**, 5071-5077.
22. P. Sandbhor Gaikwad and R. Banerjee, *Analyst*, 2018, **143**, 1326-1348.

23. S. K. Vashist, *Biosensors*, 2017, **7**, 62/61-62/64.
24. K. M. Mayer and J. H. Hafner, *Chem. Rev.*, 2011, **111**, 3828-3857.
25. J. N. Anker, W. P. Hall, O. Lyandres, N. C. Shah, J. Zhao and R. P. Van Duyne, *Nat. Mater.*, 2008, **7**, 442-453.
26. P. L. Stiles, J. A. Dieringer, N. C. Shah and R. P. V. Duyne, *Annu. Rev. Anal. Chem.*, 2008, **1**, 601-626.
27. J. R. Lombardi and R. L. Birke, *J. Chem. Phys.*, 2012, **136**, 144704.
28. Z. Mei and L. Tang, *Anal. Chem.*, 2017, **89**, 633-639.
29. J.-F. Li, C.-Y. Li and R. F. Aroca, *Chem. Soc. Rev.*, 2017, **46**, 3962-3979.
30. G. K. Joshi, K. A. Smith, M. A. Johnson and R. Sardar, *Journal of Physical Chemistry C*, 2013, **117**, 26228-26237.
31. T. Liyanage, M. Nagaraju, M. A. Johnson, B. B. Muhoberac and R. Sardar, *Nano Letters*, 2019, **20**, 192-200.
32. L. Scarabelli, M. Coronado-Puchau, J. J. Giner-Casares, J. Langer and L. M. Liz-Marzán, *ACS Nano*, 2014, **8**, 5833-5842.
33. T. Liyanage, A. Rael, S. Shaffer, S. Zaidi, J. V. Goodpaster and R. Sardar, *Analyst*, 2018, **143**, 2012-2022.
34. G. K. Joshi, S. L. White, M. A. Johnson, R. Sardar and P. K. Jain, *Journal of Physical Chemistry C*, 2016, **120**, 24973-24981.
35. G. K. Joshi, K. N. Blodgett, B. B. Muhoberac, M. A. Johnson, K. A. Smith and R. Sardar, *Nano Letters*, 2014, **14**, 532-540.
36. J. D. Driskell and R. A. Tripp, *Chemical Communications (Cambridge, United Kingdom)*, 2010, **46**, 3298-3300.
37. F. Madzharova, Z. Heiner, M. Guehlke and J. Kneipp, *Journal of Physical Chemistry C*, 2016, **120**, 15415-15423.
38. L. Qi, M. Xiao, X. Wang, C. Wang, L. Wang, S. Song, X. Qu, L. Li, J. Shi and H. Pei, *Analytical Chemistry (Washington, DC, United States)*, 2017, **89**, 9850-9856.
39. B. L. Lambert, Gronert, S., Shurvell, F. H., Lightner, A., D., 2011.
40. Z. Wang, S. Ye, N. Zhang, X. Liu and M. Wang, *Anal. Chem.*, 2019, **91**, 5043-5050.
41. B. Giese and D. McNaughton, *Phys. Chem. Chem. Phys.*, 2002, **4**, 5161-5170.
42. Y. He, X. Yang, R. Yuan and Y. Chai, *Anal. Chem.*, 2017, **89**, 8538-8544.
43. *Principles of fluorescence spectroscopy*, ed. J. Lakowicz, Springer, 3rd edn, 2006.

1  
2  
3  
4  
5  
6  
7  
8  
9  
10  
11  
12  
13  
14  
15  
16  
17  
18  
19  
20  
21  
22  
23  
24  
25  
26  
27  
28  
29  
30  
31  
32  
33  
34  
35  
36  
37  
38  
39  
40  
41  
42  
43  
44  
45  
46  
47  
48  
49  
50  
51  
52  
53  
54  
55  
56  
57  
58  
59  
60

### The Table of Contents Graphic

